Science Bulletin 68 (2023) 1514–1521

Contents lists available at ScienceDirect

Science Bulletin

journal homepage: www.elsevier.com/locate/scib

Article

Modularized batch production of 12-inch transition metal dichalcogenides by local element supply

Guodong Xue [a,1], Xin Sui [b,1], Peng Yin [c,1], Ziqi Zhou [a,1], Xiuzhen Li [d], Yang Cheng [a], Quanlin Guo [a,e], Shuai Zhang [f], Yao Wen [g], Yonggang Zuo [h], Chong Zhao [i], Muhong Wu [b,e,i], Peng Gao [b], Qunyang Li [f], Jun He [g], Enge Wang [b,i], Guangyu Zhang [d,i,*], Can Liu [c,*], Kaihui Liu [a,i,*]

[a] State Key Laboratory for Mesoscopic Physics, Frontiers Science Center for Nano-optoelectronics, School of Physics, Peking University, Beijing 100871, China
[b] International Centre for Quantum Materials, Collaborative Innovation Centre of Quantum Matter, Peking University, Beijing 100871, China
[c] Key Laboratory of Quantum State Construction and Manipulation (Ministry of Education), Department of Physics, Renmin University of China, Beijing 100872, China
[d] Beijing National Laboratory for Condensed Matter Physics and Institute of Physics, Chinese Academy of Sciences, Beijing 100190, China
[e] Interdisciplinary Institute of Light-Element Quantum Materials and Research Center for Light-Element Advanced Materials, Peking University, Beijing 100871, China
[f] Applied Mechanics Laboratory, Department of Engineering Mechanics, Tsinghua University, Beijing 100084, China
[g] Key Laboratory of Artificial Micro- and Nano-structures of Ministry of Education, Wuhan University, Wuhan 430072, China
[h] Key Laboratory of Unconventional Metallurgy (Ministry of Education), Faculty of Metallurgical and Energy Engineering, Kunming University of Science and Technology, Kunming 650032, China
[i] Songshan Lake Materials Laboratory, Dongguan 523808, China

ARTICLE INFO

Article history:
Received 19 May 2023
Received in revised form 20 June 2023
Accepted 28 June 2023
Available online 4 July 2023

Keywords:
2D materials
Batch production
300 mm wafer
Composition engineering
Heterostructures

ABSTRACT

Two-dimensional (2D) transition metal dichalcogenides (TMDs) are regarded as pivotal semiconductor candidates for next-generation devices due to their atomic-scale thickness, high carrier mobility and ultrafast charge transfer. In analog to the traditional semiconductor industry, batch production of wafer-scale TMDs is the prerequisite to proceeding with their integrated circuits evolution. However, the production capacity of TMD wafers is typically constrained to a single and small piece per batch (mainly ranging from 2 to 4 inches), due to the stringent conditions required for effective mass transport of multiple precursors during growth. Here we developed a modularized growth strategy for batch production of wafer-scale TMDs, enabling the fabrication of 2-inch wafers (15 pieces per batch) up to a record-large size 12-inch wafers (3 pieces per batch). Each module, comprising a self-sufficient local precursor supply unit for robust individual TMD wafer growth, is vertically stacked with others to form an integrated array and thus a batch growth. Comprehensive characterization techniques, including optical spectroscopy, electron microscopy, and transport measurements unambiguously illustrate the high-crystallinity and the large-area uniformity of as-prepared monolayer films. Furthermore, these modularized units demonstrate versatility by enabling the conversion of as-produced wafer-scale MoS_2 into various structures, such as Janus structures of MoSSe, alloy compounds of $MoS_{2(1-x)}Se_{2x}$, and in-plane heterostructures of MoS_2-$MoSe_2$. This methodology showcases high-quality and high-yield wafer output and potentially enables the seamless transition from lab-scale to industrial-scale 2D semiconductor complementary to silicon technology.

© 2023 Science China Press. Published by Elsevier B.V. and Science China Press. All rights reserved.

1. Introduction

The progression of semiconductor materials from the first-generation silicon-based semiconductors to third-generation wide-bandgap semiconductors represented by gallium nitride and silicon carbide, has propelled the unprecedented advancement in the semiconductor industry. However, as device miniaturization approaching its physical limits, the pace of Moore's Law is decelerating, which necessitates the exploration of novel materials to sustain the momentum of the semiconductor industry. Two-dimensional (2D) transition metal dichalcogenides (TMDs), with their ultra-thin atomic layer thickness and pristine semiconducting properties, have emerged as a compelling candidate for next-generation semiconducting channel materials [1–4]. Nevertheless, harnessing the full potential of 2D TMDs hinges on addressing

* Corresponding authors.
E-mail addresses: gyzhang@iphy.ac.cn (G. Zhang), canliu@ruc.edu.cn (C. Liu), khliu@pku.edu.cn (K. Liu).
[1] These authors contributed equally to this work.

https://doi.org/10.1016/j.scib.2023.06.037
2095-9273/© 2023 Science China Press. Published by Elsevier B.V. and Science China Press. All rights reserved.

several formidable challenges, notably the low-cost, large-scale batch production of TMDs targeting on semiconductor devices in integrated circuits (ICs).

To balance high chip yield with low-cost manufacturing, 300 mm (12-inch) silicon wafers have been adopted as the standard for semiconductor manufacturing, as proposed by the semiconductor equipment and materials international (SEMI) since 1995 [5]. To proceed with the era of 2D TMD-based semiconductors, mass production of 12-inch TMD wafers is a critical node to combine the new materials with the existing upstream and downstream manufacturing lines. Therefore, batch production of TMD wafers up to 12 inches is essential to transition TMD materials from laboratory investigations to integral components for next-generation semiconductor devices.

Over the past decade, significant advancements have been made toward producing wafer-scale TMD films [6–15]. However, their sizes are typically limited to 2 or 4 inches, and batch production capabilities remain constrained, usually limited to a single piece per batch. This restriction predominantly stems from the growth methodology of TMDs, which necessitates the simultaneous supply of chalcogen and transition metal sources in two separate temperature zones [16–20]. Since the diffusion of the two sources follows a point-to-face manner, the feedstock distribution is typically uneven along the gas transport direction [21], leading to non-uniform TMD deposition on wafers, especially for large ones. Recently, attempts at ensuring uniformity of large-scale TMD wafer are involved by vertically aligning the target wafer with the source diffusion direction [22,23]. However, this approach precludes batch production, as only one wafer can be fabricated at a time. Consequently, there is a pressing need to develop effective methods that can strike a balance between achieving large-scale uniformity and enhancing batch production capabilities.

In this work, we develop a modularized strategy to batch produce uniform TMD films with wafer sizes ranging from 2-, 4-, 8- to a record-large 12-inch. The target wafer, chalcogen, and transition metal precursor are compacted in a face-to-face manner and configured as a single module unit. In this self-sufficient system, the multi-element sources can be locally supplied and distributed evenly, ensuring the uniform growth of TMDs along the entire wafer, even for 12-inch ones. Meanwhile, by vertically stacking multiple module layers, an integrated array is formed and can further enhance the production capabilities in one batch, allowing for the success of 15 pieces per batch for 2-inch wafers and 3 pieces per batch for 12-inch wafers. Moreover, this modularized strategy also supports the versatile post-processing of batch-produced TMD wafers, enabling the creation of various structures such as Janus MoSSe, $MoS_{2(1-x)}Se_{2x}$ alloys, and MoS_2-$MoSe_2$ in-plane heterostructures.

2. Methods

2.1. Batch production of wafer-scale MoS_2

The substrates of 2- to 12-inch fused silica and sapphire (Dongda Times, Chengdu Technology Co., Ltd.) were first pretreated with O_2 plasma before the growth. Na_2MoO_4 aqueous solution (concentration: 15 mg mL^{-1}) was spin-coated on the perforated fused silica piece and heated at 80 °C for drying. The Na_2MoO_4-coated perforated fused silica, substrate and chalcogenide crystal plate (ZnS) were stacked as a growth module by the customer-designed holder. The integrated modules were placed on a quartz plate and loaded in the chemical vapour deposition (CVD) furnace. Experimentally, the batch production of 2-inch wafers was carried out in a commercial CVD furnace with a tube diameter of 120 mm and the MoS_2 growth was performed at 800 °C for 40 min. The chamber pressure was kept at ~1 Torr with 500 sccm Ar during the growth. The larger wafers (4-, 8- and 12-inch) were grown in a customized automated furnace with a tube diameter of 350 mm. The system was heated up to an optimized temperature of 820 °C and held for 60 min. The chamber pressure was kept at ~1 Torr with 800 sccm Ar during the growth. After growth, the furnace was naturally cooled down to room temperature.

2.2. Fabrication of Janus MoSSe

The Janus MoSSe structure was prepared by the postprocess of as-produced MoS_2 film on *a*-plane sapphire substrate. The as-growth MoS_2 and the ZnSe crystal plate were placed in a face-to-face manner using the customer-designed holder. This vertically integrated arrays were placed on a quartz plate and loaded into the CVD furnace. The Se substitution was performed at 870 °C and the system pressure was kept at ~1 Torr with 120 sccm Ar and 5 sccm H_2. This postprocess time was kept for 60 min and the system was naturally cooled down to room temperature after substitution. The Janus MoSSe sample was then transferred to Au substrate by etching from *a*-plane sapphire using 1 mol L^{-1} KOH solution, for further characterizations.

2.3. Fabrication of $MoS_{2(1-x)}Se_{2x}$ alloys and MoS_2-$MoSe_2$ in-plane heterostructure arrays

The $MoS_{2(1-x)}Se_{2x}$ alloys were fabricated using the as-produced MoS_2 films on *c*-plane sapphire. Similarly, the MoS_2 film and ZnSe crystal plate were stacked face-to-face using the customer-designed holder. The configuration was loaded into the CVD furnace and the substitution was processed at ~1 Torr with 120 sccm Ar and 10 sccm H_2. The substituting temperatures were at 750, 850, 950 and 1050 °C for 20%, 50%, 80% to nearly 100% Se content of $MoS_{2(1-x)}Se_{2x}$ alloys. As for the fabrication of MoS_2-$MoSe_2$ in-plane heterostructure arrays, a 50-nm-thick Al_2O_3 layer was first deposited on MoS_2 by atomic layer deposition (ALD). Then the ultraviolet (UV) lithography and phosphoric acid (H_3PO_4) etching was used to obtain different patterned Al_2O_3 mask layers. The uncovered MoS_2 was substituted to nearly $MoSe_2$ at 1050 °C for 60 min. Finally, the Al_2O_3 mask layer on the MoS_2 was etched off with H_3PO_4.

2.4. Characterizations

Optical images were taken with an Olympus BX51M microscope. Raman and photoluminescence (PL) spectra were measured by the WITec alpha300R system with a laser excitation wavelength of 514 nm and a power of ~1 mW. The atomically-resolved scanning transmission electron microscope (STEM) experiment was performed in a FEI Titan Themis G2 300 operated at 300 kV. The piezoelectric force microscopic (PFM) and high-resolution atomic force microscopic (AFM) images were acquired using an Asylum Research Cypher AFM system. The X-ray photoelectron spectroscopy (XPS) measurements were performed using an ESCALAB 250X system (Thermo Fisher Scientific) and excited by monochromatic Al Kα radiation.

2.5. Out-of-plane second harmonic generation (SHG) measurements

SHG was excited with femtoseconds pulses (Coherent laser, ~150 fs, 250 kHz) generated by a Ti:sapphire oscillator series pumping an optical parametric amplification. A collimated *p*-polarized pulsed laser beam with 2 mm spot size was guided to the objective back aperture (Nikon, 50X, NA = 0.8). The incident angle was determined by the beam position at the objective back

aperture tuned by a scanning motorized stage. The excitation wavelength was 1360 nm. We collected the SHG signal after a 750 nm short-pass filter using the same objective. To achieve the in-plane SHG extinction along the *p*-polarization of the MoSSe Janus sample, we rotated the crystal with the armchair direction perpendicular to the electric field analyzed by a polarizer.

2.6. Fabrication and measurement of MoS_2 field-effect transistor (FET)

The MoS_2 FET (W = 5 μm, L = 8 μm) was fabricated through the standard microfabrication process by electron beam lithography (EBL) techniques. The MoS_2 film was transferred onto 300 nm SiO_2/Si substrate using the polymethylmethacrylate (PMMA) film as the transfer intermediate. The Au (30 nm) contact electrodes were fabricated by electron-beam evaporation with a rate of 0.1 Å s^{-1} at ~10^{-8} Torr. Then the lift-off was carried out in acetone. The electrical measurements were performed at room temperature at a vacuum probe station (Janis) equipped with a semiconductor parameter analyser (Agilent Technologies B1500A).

3. Results and discussion

3.1. Modularized batch production of wafer-scale MoS_2

Fig. 1a depicts our experimental design for the modularized batch production of wafer-scale TMDs. In the case of MoS_2 growth, a single growth module comprises a ZnS plate (to locally supply S source), Na_2MoO_4-coated perforated fused silica (to locally supply Mo source), and a target growth substrate (sapphire or fused silica), as illustrated in Fig. 1c. This module forms a self-sufficient precursor unit for the face-to-face growth of MoS_2. At an elevated temperature of 800 °C, S monomers are released from the ZnS surface [24] and pass through the fused silica holes. Concurrently, Na_2MoO_4 vaporizes, allowing Mo source to reach the substrate surface and form monolayer MoS_2 film. Batch production is achieved by vertically stacking five module layers in the customer-designed holder, which can form an integrated production array (Fig. 1b). In this experiment, three integration arrays were loaded into a commercial CVD furnace (with a tube diameter of 120 mm) at a time and then elevated to the target temperature. As shown in Fig. 1d, 15 pieces of 2-inch uniform, clean, fully covered MoS_2 films were obtained after 40 min of growth. This modularized growth strategy would possess scalable productivity when continuously increasing the stacked modules.

Benefiting from the self-sufficient local element supply in a face-to-face manner, the as-produced MoS_2 monolayer wafers exhibit high quality and uniformity due to the efficient mass transport of multiple precursors during the growth process. The atomically-resolved STEM (Fig. 1e) and high-resolution AFM images (Fig. S1 online) show a perfect hexagonal honeycomb lattice structure formed by the Mo and S atoms, revealing the high crystallinity of as-grown MoS_2 film. The room-temperature PL peak of A exciton at ~1.84 eV has a narrow full width at half-maximum (FWHM) of 57 meV indicating its high optical quality (Fig. 1f). From the typical transfer characteristics of a MoS_2 FET device, the room temperature mobility was extracted as ~40 cm^2 V^{-1} s^{-1}, which is comparable to the devices prepared by exfoliated MoS_2 monolayers [25]. These results indicate that our modularized growth strategy is powerful in scaling up productivity without compromising the optical and electrical quality of TMD films.

3.2. Scalable production of MoS_2 wafers up to 12-inch size

This modularized design can be easily scaled up by simply enlarging the size of the furnace chamber and the corresponding modules. Here, we customized an automated CVD furnace with a tube diameter of 350 mm, capable of facilitating the mass production of significantly larger wafers (Fig. 2a). Such large furnace chamber can conveniently host wafers ranging from 2-, 4-, 8-, up to 12-inch diameter. With the aid of multiple modules, 10 pieces of 4-inch wafers, 5 pieces of 8-inch wafers, or 3 pieces of 12-inch wafers can be produced in a single batch. The as-produced MoS_2 monolayer wafers of different sizes all exhibit high optical uniformity (Fig. 2b and Fig. S2 online), benefiting from the efficient supply of multiple precursors for every wafer during the growth process.

Specifically, to check the uniformity of the 12-inch MoS_2 monolayer film (Fig. 2c), the large-scale Raman line scans along the horizontal axis and large-area mappings of the 12-inch wafer were performed (Fig. 2d and Fig. S3 online). The E_{2g} and A_{1g} characteristic peaks, located at 383 and 403 cm^{-1} respectively, both exhibit identical wavenumbers along the ~30 cm distance, confirming the exceptional uniformity throughout the entire 12-inch wafer. The statistical Raman peak distance between E_{2g} and A_{1g} was extracted to be (20.1 ± 0.3) cm^{-1}, which indicates that the deposited MoS_2 films are of uniform monolayers. Furthermore, the PL line scans across the 12-inch diameter exhibit narrow A exciton peaks located around ~1.8 eV, further affirming the optical uniformity across the entire MoS_2 wafer (Fig. 2e). Such reliable high-uniformity characteristic over such a large area of 12 inches, can be attributed to the evenly distributed feeding source facilitated by the face-to-face modularized design.

It is noteworthy that the automated equipment supports 3 to 4 growth cycle per day, thereby permitting low-cost pilot-scale MoS_2 wafer production. We anticipate that these production capabilities can be further scaled up to meet the consistent output requirements of the semiconductor industry.

3.3. Modularized substitution for Janus MoSSe monolayers

The local element supply within a single module enables precise composition engineering of as-produced wafers. As illustrated in Fig. 3a, a ZnSe plate (to locally supply Se source) and a MoS_2 film grown on *a*-plane sapphire formed a substitution module to obtain Janus MoSSe structure. At an elevated temperature of 870 °C, the top-layer S atoms gradually desorbed from the MoS_2 surface, while the bottom S atoms remain well-preserved due to the strong interaction with the *a*-plane sapphire surface [26]. Concurrently, Se monomers were released from the ZnSe plate by breaking the dangling bond, creating a localized high-concentration area of Se atoms. This facilitated frequent substitution of the top S layers, culminating in the formation of the Janus MoSSe structure. The uniform contrast of the as-prepared Janus MoSSe monolayer in the optical image (Fig. 3b) indicates the homogeneous substitution achieved through this modularized face-to-face design. Distinct from MoS_2 and $MoSe_2$ monolayers, Janus MoSSe exhibited an out-of-plane A_{1g} mode located at 289.5 cm^{-1} (due to the broken out-of-plane symmetry) and an in-plane E_{2g} mode located at 351.0 cm^{-1} (resulting from the lattice constant variation) (Fig. 3c). The representative PL peak of the as-prepared film is at 1.68 eV, in between the optical gaps of MoS_2 (1.82 eV) and $MoSe_2$ (1.55 eV), further confirming the Janus monolayer structure [27,28] (Fig. 3d).

The intrinsic broken symmetry of the Janus monolayer generates an electric polarization (P) perpendicular to the 2D surface, which will lead to a SHG response in the out-of-plane direction. By tilting the incident light at an angle of θ (Fig. 3e), the out-of-plane SHG signal can be excited by the vertical light component. As shown in Fig. 3f, the SHG intensity of Janus MoSSe increases with the tilt angle θ due to the enhancement of the vertical electric field. As a contrast, no signal is detected for randomly-distributed

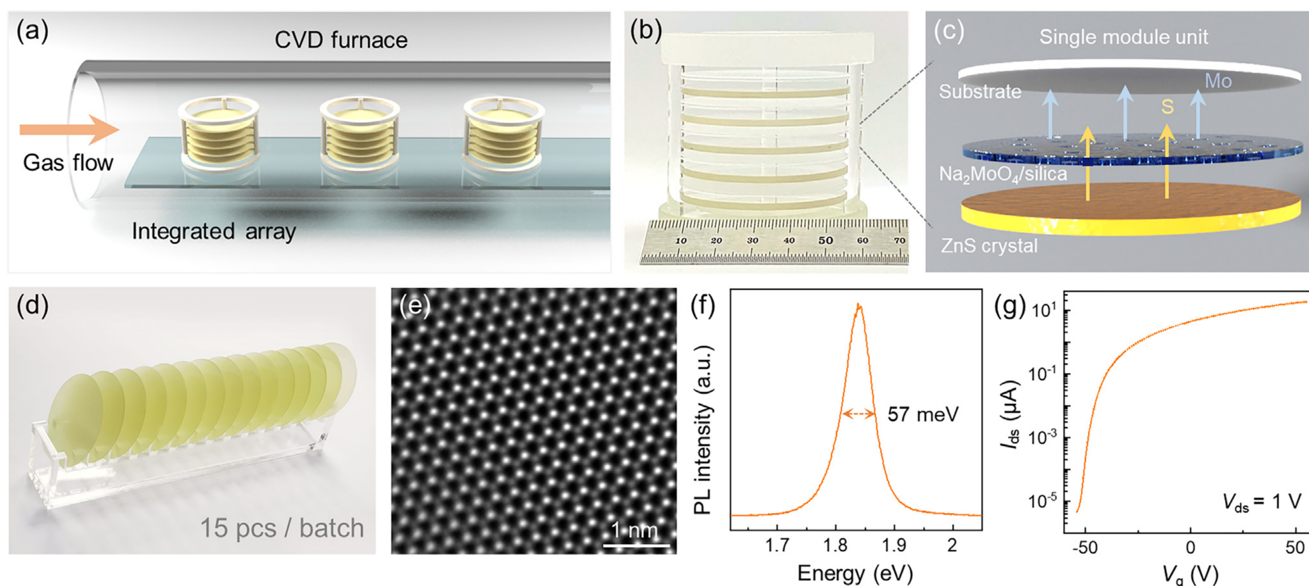

Fig. 1. (Color online) Batch production of MoS_2 wafers by the modularized strategy. (a) Schematic of the modularized design for the batch production of 15 pieces of MoS_2 wafer. (b) Photograph of the integrated arrays comprising five stacked 2-inch producing module units. (c) Schematic of a single module unit in (b) containing a ZnS plate, Na_2MoO_4-coated perforated fused silica and a target substrate. (d) Photograph of 15 pieces of MoS_2 wafer produced in one growth batch. (e) Atomically-resolved STEM image of the prepared high-quality MoS_2 film. (f) The typical room-temperature PL spectrum with a narrow FWHM of 57 meV. (g) Transfer characteristic of the MoS_2 FET with channel width of 5 μm at a bias voltage of 1 V.

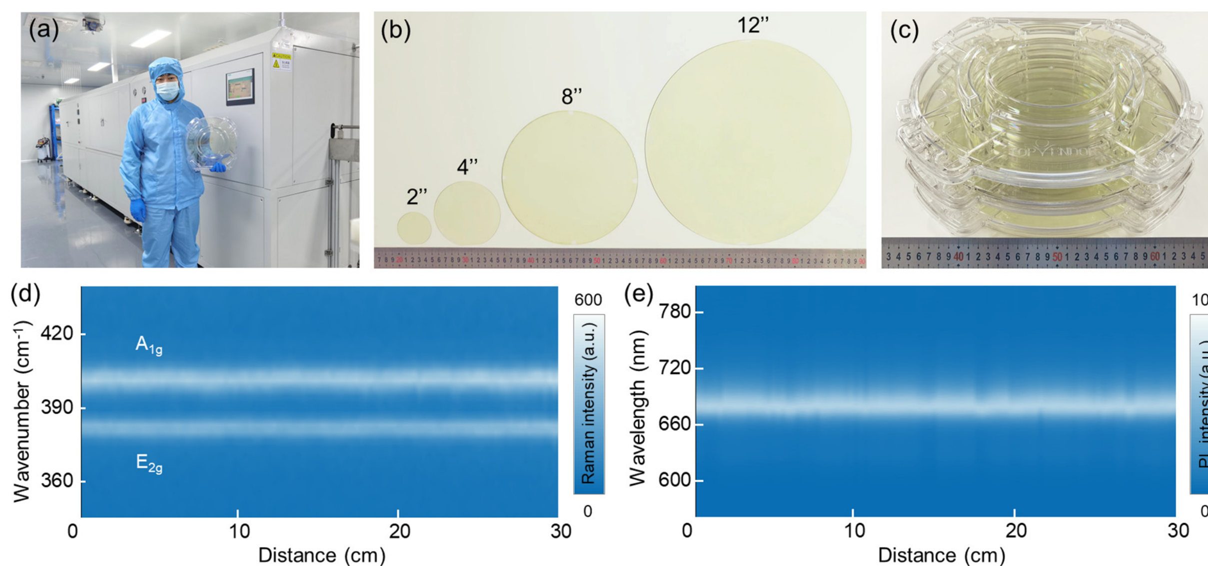

Fig. 2. (Color online) Batch production of MoS_2 wafers up to 12-inch size. (a) The customized automated CVD furnace equipment with tube diameter of 350 mm. (b) Photograph of uniform MoS_2 film with wafer sizes ranging from 2-, 4-, 8- to 12-inch. (c) Photograph of three pieces of 12-inch MoS_2 wafer produced in one batch. (d, e) Color-coded Raman (d) and PL (e) line scan mappings along the horizontal axis across the 12-inch MoS_2 wafer. The slight variations prove the uniformity of the prepared MoS_2 film.

$MoS_{2(1-x)}Se_{2x}$ alloys. These observations conclusively demonstrate the Janus structure with out-of-plane dipoles [29]. Moreover, both the A_{1g} mode Raman mapping (Fig. 3g) and the PFM image (Fig. 3h) confirm the homogeneity of the sample, signifying uniform Se substitution over a large area.

3.4. Composition engineering of wafer-scale $MoS_{2(1-x)}Se_{2x}$ alloys

The substitution module displayed remarkable flexibility in precise composition engineering of wafer-scale $MoS_{2(1-x)}Se_{2x}$ alloys. As depicted in Fig. 4a, a *c*-plane sapphire was employed as the supporting substrate for the MoS_2 monolayer substitution. Considering that the relatively weak interaction between the *c*-plane sapphire surface and the MoS_2 compared to the *a*-plane case [30], the protective effect of substrate on the bottom S layer is diminished. Therefore, the chance of S desorption and Se substitution in the bottom S layer is increased, facilitating homogeneous substitution on both sides to form wafer-scale $MoS_{2(1-x)}Se_{2x}$ alloys.

Meanwhile, the composition of alloys can be precisely modulated by controlling the substitution degree through the temperature variation. As shown in Fig. 4b, Se atoms content (x) in the post-processed TMD wafers can be conveniently tuned from 0 to nearly 100% at different activated temperatures. The quantitative Se content x is determined from the corresponding XPS spectroscopy in

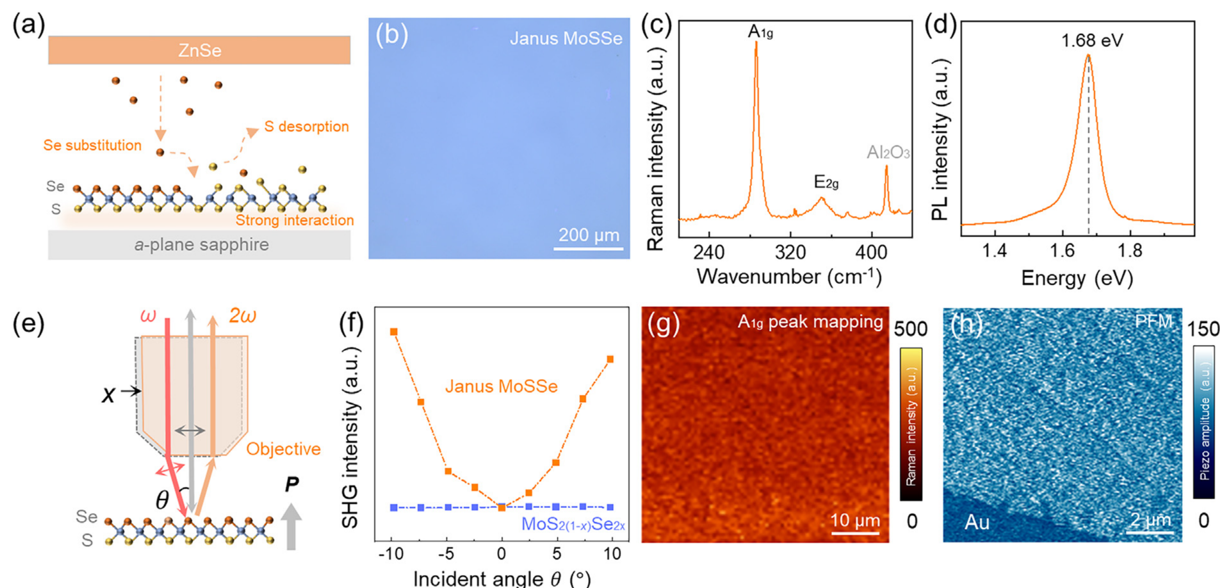

Fig. 3. (Color online) Fabrication and characterization of the Janus MoSSe. (a) Schematic of Janus monolayer fabrication by Se substituting the as-produced MoS_2 film on *a*-plane sapphire. (b) Optical image of the Janus MoSSe film. (c, d) Typical Raman (c) and PL (d) spectra of the MoSSe sample after Se substitution. (e) Schematic of the out-of-plane SHG measurement of Janus MoSSe. The incident light was tilted at an angle of θ by moving the beam position (X) at the objective back aperture using a motorized stage. (f) The out-of-plane SHG intensity evolution of Janus MoSSe and $MoS_{2(1-x)}Se_{2x}$ alloys with the incident angle θ. (g) The Raman mapping based on the A_{1g} peak intensity of the Janus MoSSe film. (h) The PFM image of the Janus MoSSe film transferred onto Au substrate.

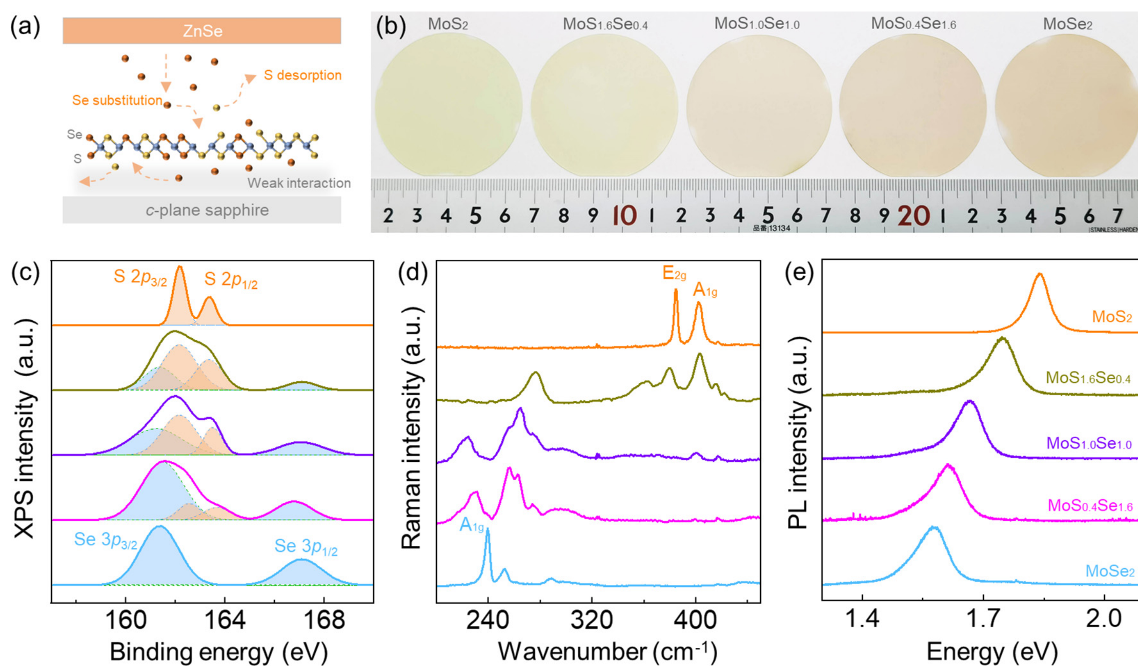

Fig. 4. (Color online) Fabrication and characterization of wafer-scale $MoS_{2(1-x)}Se_{2x}$ alloys. (a) Schematic of $MoS_{2(1-x)}Se_{2x}$ alloy fabrication by Se substituting the as-produced MoS_2 film on *c*-plane sapphire. (b) Optical image of 2-inch $MoS_{2(1-x)}Se_{2x}$ alloys with Se atoms content from 0, 20%, 50%, 80% to nearly 100% (from left to right). (c) The typical XPS spectra of MoS_2 (orange curve), $MoS_{1.6}Se_{0.4}$ (dark yellow curve), $MoS_{1.0}Se_{1.0}$ (violet curve), $MoS_{0.4}Se_{1.6}$ (magenta curve) and $MoSe_2$ (blue curve) samples in (b). The light-orange and light-blue shaded regions indicated the intensity of S and Se chemical bonding states, respectively. (d, e) The Raman and PL spectra evolution of $MoS_{2(1-x)}Se_{2x}$ alloys with variation in composition.

Fig. 4c, using the equation $x = A_{Se}/F_{Se}/(A_{Se}/F_{Se} + A_S/F_S)$ [31]. Here, A_S and A_{Se} represent the integrated peak areas of S $2p_{3/2}$ and Se $3p_{3/2}$, respectively, while F_S (0.445) and F_{Se} (0.849) denote the relative sensitivity factors for S and Se, respectively. The chemical bonding states of S $2p_{3/2}$ gradually magnified, and Se $3p_{3/2}$ diminished with the increase of Se content in alloys from 0 (orange curve), 20% (dark yellow curve), 50% (violet curve), 80% (magenta curve) to nearly 100% (blue curve). The variation in composition was further examined by the Raman spectroscopy, in which the MoS_2-featured Raman peaks attenuated and the $MoSe_2$-featured peaks gradually enhanced with the substitution evolution from MoS_2 to $MoSe_2$. Notably, the alloy samples (x = 20%, 50% and 80%) possess two new phonon modes (referred to as two-mode behavior), representing the signature of the homogeneous mixing of S and Se atoms [32,33]. Meanwhile, the PL peak exhibited a continuous redshift from 1.82 to 1.55 eV as the Se content increased (Fig. 4e). This shift

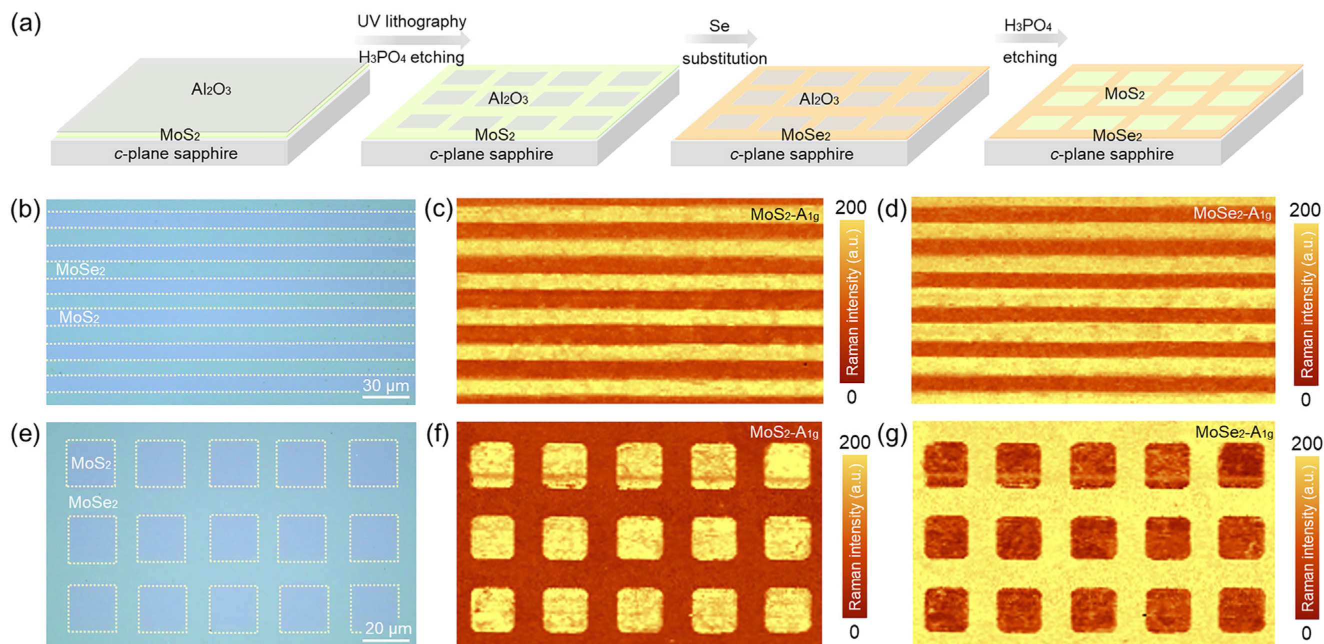

Fig. 5. (Color online) Fabrication of MoS_2-$MoSe_2$ heterostructure arrays. (a) Schematic for the spatial-selective Se substitution of MoS_2 to $MoSe_2$ using the patterned Al_2O_3 mask. (b) Optical image of the striped heterostructure patterns (with a period of 20 μm). (c, d) The Raman mapping of the striped heterostructure patterns in (b) based on the MoS_2-A_{1g} peak intensity (c) and $MoSe_2$-A_{1g} (d) peak intensity. (e) Optical image of the gridded MoS_2-$MoSe_2$ heterostructure patterns ($MoSe_2$ embedded with 20 μm MoS_2 squares). (f, g) The Raman mappings of the gridded patterns in (e) based on the MoS_2-A_{1g} (f) and $MoSe_2$-A_{1g} (g) peak intensity, respectively.

of PL position evidences the capability of this strategy for bandgaps engineering of wafer-scale TMDs through precise modulation of alloy composition.

3.5. Fabrication of MoS_2-$MoSe_2$ heterostructure arrays

The precise fabrication of large-area in-plane TMD heterostructure arrays is an essential manufacturing technique for achieving high-density integration of 2D electronic and optoelectronic devices [34–40]. Inspired by the flexible composition engineering of the as-produced MoS_2 film through the modularized Se substitution strategy, we designed diverse in-plane MoS_2-$MoSe_2$ heterostructure arrays by spatially conversion of MoS_2 to $MoSe_2$. Fig. 5a schematically illustrates the fabrication steps of MoS_2-$MoSe_2$ heterojunction by post-processing of as-produced MoS_2 films on *c*-plane sapphire. Initially, a 50-nm-thick Al_2O_3 mask layer, serving as a protective layer, was deposited on the as-produced MoS_2 by ALD. Then, a layer of photoresist was spin-coated atop the Al_2O_3 layer and subsequently patterned using UV lithography. Afterwards, the sample was immersed in H_3PO_4 to etch the photoresist unshielded regions, forming a patterned Al_2O_3 mask layer on the MoS_2 film. During the Se substitution process, the Al_2O_3 masks can efficiently protect the underlaying MoS_2 from exposure to active Se monomers. Consequently, the conversion from MoS_2 to $MoSe_2$ occurred at the unmasked regions forming sharp in-plane heterojunction interfaces. After the completion of Se substitution, the Al_2O_3 masks can be etched off in H_3PO_4.

Using the aforementioned procedure, different configurations of in-plane MoS_2-$MoSe_2$ heterostructures can be precisely produced by simply designing the Al_2O_3 mask layers. As shown in Fig. 5b, striped MoS_2-$MoSe_2$ heterostructure patterns with 20 μm periods were obtained after high temperature Se substitution, in which the $MoSe_2$ (MoS_2) exhibit a greenish (bluish) optical contrast. The Raman mapping based on the A_{1g} characteristic peaks of MoS_2 (Fig. 5c) and $MoSe_2$ (Fig. 5d) clearly delineate the outlines of heterojunction strips, thereby revealing a uniform composition distribution within each region. Moreover, another gridded MoS_2-$MoSe_2$ heterostructure pattern ($MoSe_2$ embedded with 20 μm MoS_2 squares) as shown in Fig. 5e, was fabricated by applying a squared Al_2O_3 mask layer. The Raman spectra and mappings at the embedded MoS_2 squares and surrounding $MoSe_2$ regions suggests the sharp interfaces and high quality of the gridded heterostructure arrays (Fig. 5f, g and Fig. S4 online). This spatially selective substitution of as-produced TMD film allows for the customization of pattern shapes, sizes and compositions according on demand. Meanwhile, leveraging mature microfabrication mask technology, the precision of patterning can be guaranteed, providing a practical route for designing more intricate array devices.

4. Conclusion

In this work, we developed a modularized strategy for large-scale, batch production of wafer-scale MoS_2 films. By vertically stacking multiple module layers, the production capabilities have been significantly enhanced, being capable of producing dozens of wafers per batch. Benefiting from the face-to-face local element supply, the uniform MoS_2 wafer size could be easily extended from 2-inch to a record-large 12-inch diameter. Moreover, our modularized design also showcases exceptional versatility in fabricating various TMD structures, including Janus MoSSe, $MoS_{2(1-x)}Se_{2x}$ alloys, and MoS_2-$MoSe_2$ in-plane heterostructures by the controlled Se substitution. Our strategy showed the capability of large-scale, industry-standard production of TMD wafers, and will pave a way for moving 2D electronic devices from confines of laboratory research towards the realm of high-performance applications.

Conflict of interest

The authors declare that they have no conflict of interest.

Acknowledgments

This work was supported by the National Key R&D Program of China (2022YFA1403500, 2018YFA0703700, 2022YFA1405600, and 2021YFA1202900), the National Natural Science Foundation

of China (52025023, 12274456, 51991342, 52021006, 92163206, 11888101, T2188101, 12104018, 52250398, 52203331, and 91964203), Guangdong Major Project of Basic and Applied Basic Research (2021B0301030002), the Strategic Priority Research Program of Chinese Academy of Sciences (XDB33000000), and Beijing Municipal Science and Technology Project (Z221100005822003).

Author contributions

Kaihui Liu, Can Liu, and Guangyu Zhang conceived the project; Guodong Xue, Peng Yin, and Yonggang Zuo contributed to the wafer-scale MoS_2 growth and characterizations; Xin Sui and Ziqi Zhou conducted the fabrication of Janus MoSSe, $MoS_{2(1-x)}Se_{2x}$ alloys and MoS_2-$MoSe_2$ heterostructure arrays; Xiuzhen Li, Yao Wen, and Jun He performed the electrical measurements; Yang Cheng performed the out-of-plane SHG measurements; Quanlin Guo and Peng Gao conducted the STEM characterizations; Shuai Zhang and Qunyang Li conducted the PFM characterizations; Chong Zhao and Muhong Wu assisted in setting up the customized automated CVD furnace. Important contributions to the interpretation of the results and conception were made by Kaihui Liu, Can Liu, Guangyu Zhang, and Enge Wang; all authors discussed the results and commented on the manuscript.

Appendix A. Supplementary materials

Supplementary materials to this article can be found online at https://doi.org/10.1016/j.scib.2023.06.037.

References

[1] Akinwande D, Huyghebaert C, Wang C-H, et al. Graphene and two-dimensional materials for silicon technology. Nature 2019;573:507–18.
[2] Liu C, Chen H, Wang S, et al. Two-dimensional materials for next-generation computing technologies. Nat Nanotechnol 2020;15:545–57.
[3] Das S, Sebastian A, Pop E, et al. Transistors based on two-dimensional materials for future integrated circuits. Nat Electron 2021;4:786–99.
[4] Luo P, Liu C, Lin J, et al. Molybdenum disulfide transistors with enlarged van der Waals gaps at their dielectric interface via oxygen accumulation. Nat Electron 2022;5:849–58.
[5] Hahn PO. The 300 mm silicon wafer-a cost and technology challenge. Microelectron Eng 2001;56:3–13.
[6] Chhowalla M, Shin HS, Eda G, et al. The chemistry of two-dimensional layered transition metal dichalcogenide nanosheets. Nat Chem 2013;5:263–75.
[7] Kang K, Xie S, Huang L, et al. High-mobility three-atom-thick semiconducting films with wafer-scale homogeneity. Nature 2015;520:656–60.
[8] Gao Y, Liu Z, Sun D-M, et al. Large-area synthesis of high-quality and uniform monolayer WS_2 on reusable Au foils. Nat Commun 2015;6:8569.
[9] Choi W, Choudhary N, Han GH, et al. Recent development of two-dimensional transition metal dichalcogenides and their applications. Mater Today 2017;20:116–30.
[10] Yang P, Zou X, Zhang Z, et al. Batch production of 6-inch uniform monolayer molybdenum disulfide catalyzed by sodium in glass. Nat Commun 2018;9:979.
[11] Liu C, Wang L, Qi J, et al. Designed growth of large-size 2D single crystals. Adv Mater 2020;32:2000046.
[12] Cai Z, Lai Y, Zhao S, et al. Dissolution-precipitation growth of uniform and clean two dimensional transition metal dichalcogenides. Natl Sci Rev 2020;8:nwaa115.
[13] Zeng M, Liu J, Zhou L, et al. Bandgap tuning of two-dimensional materials by sphere diameter engineering. Nat Mater 2020;19:528–33.
[14] Li T, Guo W, Ma L, et al. Epitaxial growth of wafer-scale molybdenum disulfide semiconductor single crystals on sapphire. Nat Nanotechnol 2021;16:1201–7.
[15] Wan Y, Li E, Yu Z, et al. Low-defect-density WS_2 by hydroxide vapor phase deposition. Nat Commun 2022;13:4149.
[16] Najmaei S, Liu Z, Zhou W, et al. Vapour phase growth and grain boundary structure of molybdenum disulphide atomic layers. Nat Mater 2013;12:754–9.
[17] Wang X, Gong Y, Shi G, et al. Chemical vapor deposition growth of crystalline monolayer $MoSe_2$. ACS Nano 2014;8:5125–31.
[18] Chen W, Zhao J, Zhang J, et al. Oxygen-assisted chemical vapor deposition growth of large single-crystal and high-quality monolayer MoS_2. J Am Chem Soc 2015;137:15632–5.
[19] Chen J, Zhao X, Tan SJR, et al. Chemical vapor deposition of large-size monolayer $MoSe_2$ crystals on molten glass. J Am Chem Soc 2017;139:1073–6.
[20] Zhou J, Lin J, Huang X, et al. A library of atomically thin metal chalcogenides. Nature 2018;556:355–9.
[21] Wang S, Rong Y, Fan Y, et al. Shape evolution of monolayer MoS_2 crystals grown by chemical vapor deposition. Chem Mater 2014;26:6371–9.
[22] Wang Q, Li N, Tang J, et al. Wafer-scale highly oriented monolayer MoS_2 with large domain sizes. Nano Lett 2020;20:7193–9.
[23] Zhu J, Park J-H, Vitale SA, et al. Low-thermal-budget synthesis of monolayer molybdenum disulfide for silicon back-end-of-line integration on a 200 mm platform. Nat Nanotechnol 2023;18:456–63.
[24] Zuo Y, Liu C, Ding L, et al. Robust growth of two-dimensional metal dichalcogenides and their alloys by active chalcogen monomer supply. Nat Commun 2022;13:1007.
[25] Radisavljevic B, Radenovic A, Brivio J, et al. Single-layer MoS_2 transistors. Nat Nanotechnol 2011;6:147–50.
[26] Wang J, Xu X, Cheng T, et al. Dual-coupling-guided epitaxial growth of wafer-scale single-crystal WS_2 monolayer on vicinal *a*-plane sapphire. Nat Nanotechnol 2022;17:33–8.
[27] Zhang J, Jia S, Kholmanov I, et al. Janus monolayer transition-metal dichalcogenides. ACS Nano 2017;11:8192–8.
[28] Guo Y, Lin Y, Xie K, et al. Designing artificial two-dimensional landscapes via atomic-layer substitution. Proc Natl Acad Sci USA 2021;118:e2106124118.
[29] Lu A-Y, Zhu H, Xiao J, et al. Janus monolayers of transition metal dichalcogenides. Nat Nanotechnol 2017;12:744–9.
[30] Wang Q, Tang J, Li X, et al. Layer-by-layer epitaxy of multi-layer MoS_2 wafers. Natl Sci Rev 2022;9:nwac077.
[31] Lim YR, Han JK, Yoon Y, et al. Atomic-level customization of 4 in. transition metal dichalcogenide multilayer alloys for industrial applications. Adv Mater 2019;31:1901405.
[32] Mann J, Ma Q, Odenthal PM, et al. 2-Dimensional transition metal dichalcogenides with tunable direct band gaps: $MoS_{2(1-x)}Se_{2x}$ monolayers. Adv Mater 2014;26:1399–404.
[33] Xie LM. Two-dimensional transition metal dichalcogenide alloys: preparation, characterization and applications. Nanoscale 2015;7:18392–401.
[34] Gong Y, Lin J, Wang X, et al. Vertical and in-plane heterostructures from WS_2/MoS_2 monolayers. Nat Mater 2014;13:1135–42.
[35] Huang C, Wu S, Sanchez AM, et al. Lateral heterojunctions within monolayer $MoSe_2$-WSe_2 semiconductors. Nat Mater 2014;13:1096–101.
[36] Mahjouri-Samani M, Lin M-W, Wang K, et al. Patterned arrays of lateral heterojunctions within monolayer two-dimensional semiconductors. Nat Commun 2015;6:7749.
[37] Zhang Z, Chen P, Duan X, et al. Robust epitaxial growth of two-dimensional heterostructures, multiheterostructures, and superlattices. Science 2017;357:788–92.
[38] Rao G, Wang X, Wang Y, et al. Two-dimensional heterostructure promoted infrared photodetection devices. InfoMat 2019;1:272–88.
[39] Zhang Z, Huang Z, Li J, et al. Endoepitaxial growth of monolayer mosaic heterostructures. Nat Nanotechnol 2022;17:493–9.
[40] Liu C, Liu K. Monolayer mosaic heterostructures. Nat Nanotechnol 2022;17:439–40.

Guodong Xue is currently a doctoral candidate at Peking University. He received his B.S. degree from the University of Electronic Science and Technology of China in 2021. His research interest includes the growth, characterization and application of 2D TMDCs.

Xin Sui is currently a doctoral candidate at Peking University. He received his B.S. degree from Lanzhou University in 2022. His research interest includes the growth, characterization and application of anisotropic 2D materials.

Peng Yin is currently a master candidate at Renmin University of China. He received his B.S. degree from University of Science and Technology Beijing in 2022. His research interest includes the design growth, regulation and control of 2D Van der Waals materials.

Can Liu is currently a principle investigator at Renmin University of China. She received her B.S. degree from Northwestern Polytechnical University in 2014 and her Ph.D. degree from Peking University in 2019. From 2019 to 2022, she worked as a postdoctoral fellow at Peking University. Her research interest includes the interfacial modulation growth of single-crystal 2D materials and their optical characterizations.

Ziqi Zhou is currently a postdoctoral fellow at Peking University. She received her B.S. degree from Lanzhou University in 2015, and her Ph.D. degree from the Institute of Semiconductor, Chinese Academy of Sciences, in 2021. Her research interest includes the growth, electric engineering, and optoelectronics of low-dimensional semiconductors.

Kaihui Liu is currently a professor at the State Key Laboratory for Mesoscopic Physics, School of Physics, Peking University. He received his B.S. degree from Beijing Normal University and his Ph.D. degree from the Institute of Physics, Chinese Academy of Sciences in 2009. Afterward he worked as a postdoctoral fellow at UC Berkeley, USA, until 2014. His current research interest is the growth and device physics of meter-scale single crystals including single-crystal copper foils, graphene, TMDCs, and 2D materials optical fiber.

Guangyu Zhang is currently a professor at Beijing National Laboratory for Condensed Matter Physics and Institute of Physics, Chinese Academy of Sciences. He is also the deputy director of Songshan Lake Materials Laboratory in Guangdong. He received his B.S. degree from Shandong University in 1999 and his Ph.D. degree from the Institute of Physics, Chinese Academy of Sciences in 2004. From 2004 to 2008, he worked as a postdoctoral fellow at Stanford University. His current research interest is low dimensional (especially 2D) materials with focusing on their novel electronic and mechanical properties and related device applications.